Taylor & Francis
Taylor & Francis Group

Combustion Science and Technology

ISSN: (Print) (Online) Journal homepage: https://www.tandfonline.com/loi/gcst20

Comprehensive Analyses on the Influential Factors in Supersonic Combustion Simulation Using Dynamic Adaptive Chemistry Method

Kun Wu, Francesco Contino & Xuejun Fan

To cite this article: Kun Wu, Francesco Contino & Xuejun Fan (2022): Comprehensive Analyses on the Influential Factors in Supersonic Combustion Simulation Using Dynamic Adaptive Chemistry Method, Combustion Science and Technology, DOI: 10.1080/00102202.2022.2115838

To link to this article: https://doi.org/10.1080/00102202.2022.2115838

Published online: 31 Aug 2022.

COMBUSTION SCIENCE AND TECHNOLOGY
https://doi.org/10.1080/00102202.2022.2115838

Taylor & Francis
Taylor & Francis Group

Comprehensive Analyses on the Influential Factors in Supersonic Combustion Simulation Using Dynamic Adaptive Chemistry Method

Kun Wu[a], Francesco Contino[b], and Xuejun Fan[a,c]

[a]State Key Laboratory of High Temperature Gas Dynamics, Institute of Mechanics, Chinese Academy of Science, Beijing, People's Republic of China; [b]Institute of Mechanics, Materials and Civil Engineering (iMMC), Université catholique de, Louvain (UCLouvain), Belgium; [c]School of Engineering Science, University of Chinese Academy of Sciences, Beijing, People's Republic of China

ABSTRACT

To overcome the major challenge of reactive flow simulation for chemical kinetics dominated flame dynamics in supersonic combustion, on-the-fly mechanism reduction for high fidelity simulation of scramjet becomes mandatory. For dynamic adaptive chemistry (DAC) methodology, there are three major factors controlling the accuracy and efficiency of the overall simulation, namely, the mechanism reduction method, error threshold value ε_{DAC}, and search initiating species (SIS). In the present work, systematic investigations of the three influential factors were conducted for large eddy simulation of ethylene-fueled supersonic combustion within a unified DAC framework. The results show that all the four mechanism reduction methods, i.e., DRG, DRGEP, PFA, and DAC-L, are adequate for the combustor's global performance prediction regarding the wall pressure, stable combustion productions, and temperature. However, for intricate flame stabilization characteristics, the DRG, DRGEP, and DAC-L methods yield comparable prediction accuracy in radical distributions, whereas the PFA method leads to relatively large discrepancies compared to direct integration with the detailed mechanism. The DRGEP method obtains the best balance between numerical accuracy and computational efficiency among the four methods, while the PFA method is the most computationally demanding one. Regarding the mechanism reduction error threshold value, the relative errors in physical property predictions increase as the relaxation of the error threshold value. And the comparative study suggests that the ε_{DAC} should not exceed 10^{-4} for high fidelity simulations of supersonic combustion. Furthermore, the stable species combination, namely, fuel, O_2, and N_2 incurs larger relative errors in radical mass fraction prediction than the combination including fuel and intermediate species HO_2 and CO. Nevertheless, the latter is less computationally efficient than the former as it requires 15% more CPU time to solve the stiff ODE system of the resultant skeletal mechanism. It should be noted that the computational overheads for mechanism reduction under various ε_{DAC} values and SIS combinations are almost the same, and the overall computational efficiency is mainly determined by the CPU time for solving the stiff ODE system of the size-reduced skeletal mechanisms.

ARTICLE HISTORY
Received 15 May 2022
Revised 15 August 2022
Accepted 18 August 2022

KEYWORDS
Dynamic adaptive chemistry; mechanism reduction method; error threshold; search initiating species; High-fidelity numerical simulation

CONTACT Xuejun Fan xfan@imech.ac.cn State Key Laboratory of High Temperature Gas Dynamics, Institute of Mechanics, Chinese Academy of Science, Beijing 100190, People's Republic of China

Introduction

Hypersonic air-breathing propulsion technology has gained increasing attentions in the past few decades, and one of the enabling technologies is the development of propulsion systems capable of operating across an extended range of Mach number (Ma) (Bertin and Cummings 2003). Consequently, extending the limiting operation condition and enhancing the combustion efficiency of supersonic combustion ramjet engine (scramjet) raise challenges to the research of reliable ignition and robust flame stabilization in supersonic flow (Urzay 2018). Theoretically, it is undoubted that accurate prediction of transient flame dynamics requires appropriate modeling of detailed chemical kinetics as its prerequisite (Law et al. 2003). Nevertheless, comprehensive chemical kinetic mechanisms for realistic fuels often incorporate reaction pathways valid over a wide range of operating conditions and typically involve hundreds of species and thousands of elementary reactions, which are inhibitive for high fidelity simulations (Fureby 2012; Lu and Law 2009).

However, for most practical combustion problems, a relatively smaller number of species and reactions dominate the pivotal combustion characteristics such as flame propagation and heat release. This observation leads to the mechanism reduction approaches that eliminate redundant species and reactions from the full mechanisms (Lu and Law 2005). Most methods reduce the full mechanism to a single skeletal mechanism, either by defining a problem-specific merit function or generating reduced sub-mechanisms at a group of sampled conditions, which is also known as static skeletal mechanism. The static skeletal mechanism strategy has enjoyed its popularity for a long time in supersonic combustion simulations (Hitch and Lynch 2009; Potturi and Edwards 2015; Yao 2019; Zhong et al. 2013) owing to high computation efficiency.

However, recently Wu, Yao, and Fan (2017a) revealed that the static skeletal mechanism approach is insufficient for flame dynamics prediction in scramjet engines. As the static skeletal mechanisms are generated before reactive flow simulations, their feasibility ranges can hardly cover the diverse thermochemical conditions encountered for most transient problems. Essentially, this deficiency of the static skeletal mechanism approach is inherited from the separation of mechanism reduction and fluid dynamic simulation, since the entire thermochemical space is unknown a priori. To this end, Liang, Stevens, and Farrell (2009a) proposed the dynamic adaptive chemistry (DAC) methodology, in which the adaptively reduced mechanisms were rigorously valid for their local and instantaneous thermochemical conditions with only minor computational overheads. This procedure removes redundant species from the detailed mechanism and freezes their mass fractions in the subsequent calculation, resulting in a reduced ODE system thus accelerates the computation. Basically, the performance and accuracy of the DAC scheme depend on the reduction method utilized, the search initiating species (SIS) chosen, and the error threshold value specified (Wei et al. 2017; Zhou and Wei 2016).

To minimize the computational overhead for mechanism reduction during the running time, mechanism reduction methods that scale linearly with the problem size are typically used in the DAC scheme. Tosatto, Bennett, and Smooke (2013) formulated a DRG-based DAC scheme, which achieves speedup factor of 5 and 10 for steady JP-8 flame and a transient ethylene flame, respectively. Yang et al. (2013) combined the DAC scheme with the DRG method in turbulent methane flame simulation and accurately reproduced the combustion process of a partially stirred reactor. Liang et al. paired a modified version of

the DRGEP (Pepiot-Desjardins and Pitsch 2008) in DAC (denoted as DAC-L hereinafter) for single-cell HCCI (Homogeneous-Charge Compression Ignition) (Liang, Stevens, and Farrell 2009a) engine and homogeneous auto-ignition simulations (Liang et al. 2009b) to achieve more than 30-fold speedup with high accuracy. Contino et al. (2011, 2013, 2014) also utilized the DRGEP-based DAC to investigate the nitric oxide effect on the ignition of iso-octane in a single-cylinder HCCI engine, which gained a speed-up factor up to 1500 when coupled DAC with ISAT. Gou et al. (2013) paired the PFA (Sun et al. 2010) method with the DAC scheme with error control and obtained 5–100 fold speedup with high accuracy. By combining an element flux analysis (EFA) method with the DAC scheme, He, Androulakis, and Ierapetritou (2010) achieved a 25-fold speedup in a simulation of *n*-pentane in a pairwise mixed stirred reactor, nonetheless the overhead of flux-based reduction method consumed nearly 20% of the total computational time. As a systematic assessment, Li et al. (2018) demonstrated that the DRGEP, DAC-L, and EFA models are more superior in performance compared to the DRG and PFA models in moderate or intense low-oxygen dilution (MILD) combustion.

To control the accuracy and efficiency of the DAC scheme, an appropriate error threshold value ε_{DAC} for mechanism reduction is generally determined by user knowledge or trial and error. However, this could be challenging since there is no direct relation between the model reduction threshold and the error of the resultant skeletal mechanism. To this end, Gou et al. (2013) devised a PFA-based DAC scheme with error control, in which data tabulated from zero-dimensional calculations were combined with progress variables to automatically determine appropriate error thresholds during the simulation. Despite its high speedup factor (5–100 folds), the tabulated data and choice of reaction progress variables may lack generality in turbulent combustion simulations. Thus, a new DAC scheme that concerns solution error control was formulated by Oluwole et al. (2015) and proven to be as fast as DRG model in zero-dimensional auto-ignition and two-dimensional laminar flame calculations. Besides, Xie et al. (2017) improved the accuracy in ignition delay time and composition calculation of DRG-based DAC by introducing a Jacobian-aided rate analysis to control the solution error.

Finally, apart from the mechanism reduction method and reduction error threshold, the selection of SIS is among the other major factors controlling the performance and accuracy of DAC scheme. Traditionally, SIS are chosen based on their expected importance to key combustion process. Typical choices of SIS include the fuel, oxygen, combustion products (e.g., CO_2), and necessary radicals or intermediate species (e.g., H, OH, CO, HO_2). The original DRG method (Lu and Law 2005) initiates the search with fuel or oxidizer; however, Liang, Stevens, and Farrell (2009a) found that the fuels fails to connect to any other species in the post-ignition stage in the DAC scheme, which necessitates the inclusion of CO and HO_2 in the SIS as [Fuel, CO, HO_2]. Meanwhile, for mechanism reduction with the DRGEP method, Niemeyer, Sung, and Raju (2010) using the hydrocarbon parent fuel, O_2, and N_2 as SIS [Fuel, O_2, N_2] worked well. In an attempt to follow the reaction progress, Shi et al. (2010) proposed an extended DAC (E-DAC) scheme that switches between a small numbers of SIS sets based on local thermochemical state, yielding an additional 8–10% time saving in a three-dimensional simulation for *n*-heptane combustion. However, the E-DAC scheme utilizes only a given number of SIS sets, hence its accuracy will suffer if combustion conditions are encountered where none of the SIS is appropriate. As such, Curtis, Niemeyer, and Sung (2015) developed a method to automatically determine appropriate SIS for

DRGEP-based DAC scheme, which solely relies on the local thermochemical state, namely, the relative important index.

Originated from the tackling of complex chemistries involved in internal combustion engines, the application of DAC scheme in scramjet engine is not straightforward and its efficacy is not sufficiently evaluated. This can be attributed to the fact that the convection and diffusion process are more significant due to heterogeneous combustion in scramjet engines, which is regarded as mixing controlled combustion. In our previous work, A DRGEP-based DAC scheme was exploited in ethylene-fueled supersonic combustion simulation and just preliminarily demonstrated the balanced capability in accurate prediction of flame stabilization and computation efficiency (Wu et al. 2018). Nevertheless, it would be better to consider this work as a proof-of-concept of DAC in supersonic combustion, while a systematic investigation on the influential factors for DAC simulation of scramjet relevant conditions is still lacking. This motivated us to conduct a comprehensive study to formulate heuristic guidelines for DAC simulation for the supersonic combustion community. Therefore, the present work is to provide a comprehensive assessment of the DAC scheme under supersonic combustion conditions, covering all the aforementioned performance-affecting factors such as the mechanism reduction method, the reduction error threshold, and SIS.

Large eddy simulation will be conducted with four different mechanism reduction methods against a benchmark case using the detailed ethylene oxidation mechanism (57-species, 269-reactions) ("Chemical-Kinetic Mechanisms for Combustion Applications"). It should be noted that, as reviewed recently by Yao (2019), the scales of the chemical mechanisms are restricted to 50 species for the state-of-the-art high-fidelity simulations of supersonic combustion with hydrocarbon fuels. Therefore, the present employed chemistry is a representative scale of the chemical mechanisms involved in supersonic combustion simulations. To assess the capability of the DAC under various configurations, comprehensive comparisons will be given regarding fluid flow characteristics, combustors global efficiencies, and flame dynamics. The paper is outlined as follows. First, Section 2 outlines the formulation and framework of the DAC method in more details. Then, the experimental configuration, numerical methodology, and associated simulation setup for the supersonic combustion baseline are elaborated in Section 3. Influences of the mechanism reduction method, error threshold value, and SIS on the numerical accuracy and computational efficiency of the DAC simulations are systematically discussed in Section 4. Finally, conclusions are given in Section 5.

Dynamic adaptive chemistry algorithm

Framework of the dynamic adaptive chemistry scheme

In finite-rate chemistry framework, each computational cell is treated as an individual chemistry problem with pressure, temperature, and species mass fractions comprised in a thermochemical state vector $\boldsymbol{\phi} = \boldsymbol{\phi}(p, T, Y_1, Y_2 \ldots Y_{Ns})$. Most reacting flow solvers rely on an operator splitting method: transport term and chemical source term are solved sequentially. Generally, the computational effort for solving these stiff ODEs scales at least with the square of the number of species, which becomes remarkable for large-scale combustion simulation with complex hydrocarbon fuels. As for the simulations with DAC scheme, the

full chemistry mechanism is first reduced to a skeletal mechanism with N_{asp} active species (denoted by superscript a), and N_{isp} inactive species (denoted by superscript i). As a result, the chemical source terms are formulated by a set of stiff ODEs:

$$\begin{bmatrix} \dot{y}_1^a \\ \vdots \\ \dot{y}_{N_{asp}}^a \\ \dot{T} \end{bmatrix} = \begin{bmatrix} f_1\left(p, T, y_1^a \ldots y_{N_{asp}}^a, y_1^i \ldots y_{N_{isp}}^i\right) \\ \vdots \\ f_{N_{asp}}\left(p, T, y_1^a \ldots y_{N_{asp}}^a, y_1^i \ldots y_{N_{isp}}^i\right) \\ f_{N_{asp}+1}\left(p, T, y_1^a \ldots y_{N_{asp}}^a, y_1^i \ldots y_{N_{isp}}^i\right) \end{bmatrix} \tag{1}$$

where p denotes the pressure, T the temperature, y_k^a the mass fraction of the kth active species, and y_m^i the mass fraction of the mth inactive species, respectively. To minimize the size of the ODE system while accounting for the third-body and pressure-dependent reactions, the concentrations of the inactive species are still considered when evaluating the chemical source terms (Contino et al. 2011). The DAC scheme does this reduction on-the-fly for each local and instantaneous thermochemical condition encountered, and expedite the simulation by solving a downsized stiff ODE system.

Mechanism reduction methods

To assess various chemical mechanism reduction methods within the on-the-fly reduction framework, four approaches including the DAC-L (Liang, Stevens, and Farrell 2009a), DRG (Lu and Law 2005), DRGEP (Pepiot-Desjardins and Pitsch 2008), and PFA (Sun et al. 2010) are considered in the present work. Among all these methods, the DRG method serves as the backbone, which is based on a graph representation of the reaction network and establishes the linkage between various species with weighted factors. As schematized in Figure 1, each vertex represents a species in the full mechanism and each directed edge denotes the immediate dependence of one species to another. The interaction coefficient r_{AB} quantities the contribution of species B to the production rate of species A:

$$\varepsilon = r_{AB} = \frac{\sum_{i=1,n_R} \left|\upsilon_{A,i}\omega_i\delta_{Bi}\right|}{\sum_{i=1,n_R} \left|\upsilon_{A,i}\omega_i\right|} \tag{2}$$

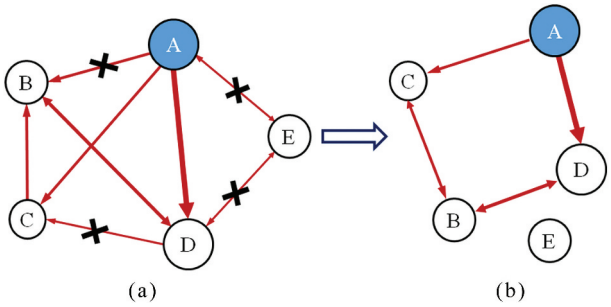

Figure 1. Schematic diagram of a directed relation graph: (a) before dimensional reduction; (b) after dimensional reduction with species A being considered to be the search initiating species.

where $\upsilon_{A,i}$ is the stoichiometric coefficient of species A in reaction i, ω_i denotes the production rate of reaction i, n_R the total number of reactions and δ_{Bi} is defined as:

$$\delta_{Bi} = \begin{cases} 1, & \text{if the } i \text{ th reaction involves species B} \\ 0, & \text{otherwise} \end{cases} \tag{3}$$

Obviously, r_{AB} measures the normalized error of the production rate of species A incurred by the elimination of all the reactions that involve species B. Then a directed relation graph is constructed by a search procedure in which there is a directed edge from A to B if and only if r_{AB} exceeds or equal to a certain threshold value as displayed in Figure 1b.

Regarding the definition of dependencies between species, Pepiot-Desjardins and Pitsch (2008) argued that a more accurate way is to evaluate the production and consumption separately instead of the net contribution, as in the directed relation graph with error propagation method (DRGEP):

$$r_{AB} = \frac{\left|\sum_{i=1,n_R} \upsilon_{A,i}\omega_i\delta_{Bi}\right|}{\max(P_A, C_A)} \tag{4}$$

in which P_A and C_A represent the production and consumption rates of species A, respectively, which are expressed with:

$$P_A = \sum_{i=1,n_R} \max\left(0, \upsilon_{A,i}\omega_i\right) \tag{5}$$

and

$$C_A = \sum_{i=1,n_R} \max\left(0, -\upsilon_{A,i}\omega_i\right) \tag{6}$$

In the DRGEP method, the effect of removing species group is also included, since the previously removed species are considered recursively. In contrast to the DRG method, the DRGEP incorporates the notion of error propagation in evaluating the error r_{AB} which takes the length of the path the error has to propagate into account:

$$r_{AB,p} = \prod_{i=1}^{n-1} r_{S_iS_{i+1}} \tag{7}$$

where $S_1 = A$, $S_2 = B$ and p denote a certain path that links species A and B while the overall error ε can be calculated as:

$$\varepsilon = r_{AB} = \max_{allpathp} r_{AB,p} \tag{8}$$

By definition, the DRG and DRGEP methods build upon the absolute and net reaction rates for active species selection. However, the use absolute reaction rates in DRG makes the relation index not conservative, while DRGEP only picks up the strongest reaction path which cannot identify the species flux physically. Thus, based on a production and consumption fluxes instead of the level of interactions between species, Sun et al. (2010) proposed the path flux analysis (PFA) method.

By following Eqns. (5) and (6), the fluxes of species A related with species B can be calculated as:

$$P_{AB} = \sum_{i=1,n_R} \max\left(0, v_{A,i}\omega_i\delta_{Bi}\right) \tag{9}$$

$$C_{AB} = \sum_{i=1,n_R} \max\left(0, -v_{A,i}\omega_i\delta_{Bi}\right) \tag{10}$$

To introduce the flux information, Sun et al. (2010) defined a new contribution coefficient that includes both direct links (first generation) and indirect links through a third species (second generation). Specifically, the contribution coefficient of first generation is defined as:

$$r_{AB}^{P-1st} = \frac{P_{AB}}{\max(P_A, C_A)} \tag{11}$$

$$r_{AB}^{C-1st} = \frac{C_{AB}}{\max(P_A, C_A)} \tag{12}$$

The corresponding contribution coefficient of the second generation, which measures the flux ratios between A and B via third reactant M_i, is defined as:

$$r_{AB}^{P-2nd} = \sum_{M_i \neq A,B} \left(r_{AM_i}^{P-1st} r_{M_iB}^{P-1st} \right) \tag{13}$$

$$r_{AB}^{C-2nd} = \sum_{M_i \neq A,B} \left(r_{AM_i}^{C-1st} r_{M_iB}^{C-1st} \right) \tag{14}$$

Subsequently, the overall coefficient of PFA is aggregated as:

$$r_{AB} = r_{AB}^{P-1st} + r_{AB}^{C-1st} + r_{AB}^{P-2nd} + r_{AB}^{C-2nd} \tag{15}$$

As the computational cost increases exponentially with the generations, thereby only two generations are considered in the present work.

The DAC-L method employed in the present study was first proposed by Liang, Stevens, and Farrell (2009a) based on a modified DRGEP method by neglecting the influence of removing a species group. It should be noted that in the original DAC-L method (Liang, Stevens, and Farrell 2009a), Fuel, CO, and HO_2 were selected to initiate the reduction process. However, it was found that these species do not equally contribute to the system reactivity throughout the simulation. As such, Shi et al. (2010) improved the DAC-L by introducing two progress variables to quantify the combustion status. The first variable is the progress equivalence ratio to indicate the inclusion of fuel in the SIS, while the traditional equivalence ratio to estimate the completeness of the combustion. Since the progress equivalence ratio is more beneficial for large-scale hydrocarbon fuels, we resorted to the traditional DAC-L for ethylene-air combustion in the present work while the improved DAC-L will be investigated in our future study.

Search-Initiating species

In DRG-like method, species deemed of primary importance are selected as SIS whereby a search is performed to identify the set of species on which these initiating species depend. The mechanism reduction procedure is equivalent to identifying vertices to which there exist strong paths connecting them to a vertex in the search initiating species set. The union of the subsidiary sets form the active species set of the resultant-reduced mechanism.

Typically, reactions in oxidation mechanism of large hydrocarbon fuels can be classified into three interacting groups (1) hydrocarbon decomposition, (2) H_2-O_2 reaction system, and (3) CO oxidation reaction system. Correspondingly, search-initiating species have been chosen based on their expected importance to these chemical reaction groups. Typical choices of target species include the fuel, oxygen, combustion products (e.g., CO_2 and H_2O), certain key radicals and intermediate known to be good indicator species (e.g., HO_2 and CO). Therefore, to demonstrate the effect of SIS on the performance of DAC, two commonly used combinations: (1) SIS involving only stable species as fuel, O_2, and N_2 (denoted as Stable-SIS), (2) SIS consisting of fuel, intermediate species HO_2, and CO (denoted as Inter-SIS).

Simulation configuration and numerical methodology

Description of the experiment configuration

The validation benchmark is taken from the experiment conducted by Situ et al. (1999) in a directly connected pipe test rig. The quasi two-dimensional combustor is 1100 mm in length with a rectangle inlet of 65 mm in height and 40 mm in width. As shown in Figure 2, a 370-mm-long mixing section is followed by a 3.6° unilateral expansion section till the combustor exit. The incoming vitiated air supplied by burning hydrogen in air with oxygen replenishment has a raised stagnation pressure of 0.09977 MPa and temperature of 1700 K. The vitiated air is composed of 71.5% N_2, 23.3% O_2, and 5.2% H_2O in mass fraction. The fuel stream is supplied with the hot products of kerosene/air combustion at Ma 1.25 in an upstream subsonic combustor. Since the products' exact composition is not available, thereby it is determined based on a simplified chemistry model (Situ et al. 1999). Gaseous ethylene is considered as the surrogate to represent the main product of the kerosene pyrolysis after initial endothermic reactions (Molvik, Bowles, and Huynh 1992). Then, the composition of the hot fuel-rich products is obtained based on a one-step global reaction by matching the combustion efficiency derived from measured total temperature and pressure at the upstream subsonic combustor exit. In the experiment, both air and fuel streams were axially injected into the supersonic combustor which was separated by a 6-mm-high plate. The experimental operation conditions specifying the compositions

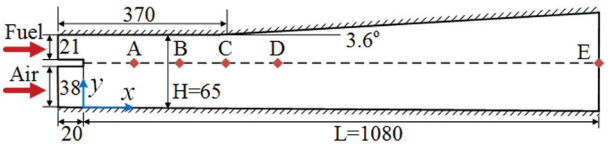

Figure 2. Numerical configuration of the model supersonic combustor.

Table 1. Experimental operating conditions for both vitiated air and fuel streams.

Parameter	P [MPa]	Ma	T [K]	Y_{N2}	Y_{O2}	Y_{C2H4}	Y_{H2O}	Y_{CO2}
Air	0.0977	2.15	491.9	0.7150	0.2330	0.0	0.0520	0.0
Fuel	0.1731	1.25	1771.9	0.6067	0.0103	0.1059	0.1566	0.1205

of both the vitiated air and fuel streams are summarized in Table 1. During the experiment, static wall pressures were measured by 23 pressure taps on the lower wall and 13 taps on the upper wall, respectively.

Numerical models and algorithm

To assess the effect of various influential factors in DAC simulation of flame stabilization phenomenon, it is necessary to leverage the large eddy simulation to capture the fluid dynamics and mixing on the small-scale vortices. In this section, only a brief summary will be given regarding the physical models and numerical algorithms used in the present study, and more details can be found in our previous works (Wu et al. 2017b; Wu, Zhang, and Fan 2022). The Favre filtered conservation equations for mass, momentum, energy and species are solved. The laminar viscosity is obtained by Sutherlands law, while the thermal and mass diffusion coefficients are calculated by assuming constant Prandtl and Schmidt numbers. The subgrid turbulent viscosity is obtained via the one-equation turbulence model, in which a transport equation of the subgrid kinetic energy is solved (Yoshizawa 1986). The filtered reaction rates, resulted from the turbulence-chemistry interaction, are modeled using a multi-scale subgrid turbulent combustion model, namely, partially stirred reactor model (PaSR) (Karlsson 1995).

The time discretization was handled with the second-order Crank-Nicholson scheme and second-order TVD (total variation diminishing) scheme was used for spatial discretization. The resultant equation system was solved by an in-house solver developed based on the OpenFOAM platform (Wu et al. 2017b, 2018; Wu, Yao, and Fan 2017a; Wu, Zhang, and Fan 2022).

Numerical setup

The computational model is shown in Figure 2, where the streamwise and transverse coordinates $\hat{x}$ and $\hat{y}$ are normalized by the combustor length L and height H, respectively. The computational model spans one-twentieth (2 mm) of its real width in the spanwise direction resembling the quasi two-dimensional characteristics. The computational grid was generated with block-structured hexahedral cells and local refinements were clustered around the shear layer emanating from the split plate. The shear layer where flame stabilizes is resolved by 61 transverse grid points to capture the turbulent mixing and combustion. The mean and maximum grid sizes in the mixing zone are 0.2 mm and 0.35 mm, respectively. Since the main reaction zone under the present combustor configuration is far away from the combustor walls, it is therefore modeled by slip condition to alleviate the grid resolution requirement near the wall. The grid convergence study has been conducted in our previous work based on three levels of grid refinement (Wu, Yao, and Fan 2017a), and

the present study employs the 0.28 million one as a balance between numerical accuracy and computation cost.

Regarding the boundary conditions, fixed pressure, temperature and species composition are specified according to those in Table 1 at both air and fuel inlets. Turbulent-like inlet is imposed for the velocity inlet boundary in which the mean profile is modulated by white noise perturbation with 5% of its magnitude. Supersonic outflow boundary condition is applied to the combustor exit for all variables. The computational time step is constrained by a maximum Courant number of 0.3 to ensure numerical stability. A typical simulation takes 12 flow-through times ($t_f = L/U_\infty$), among which $8t_f$ are needed to reach the quasi steady state followed by another $4t_f$ for data sampling and statistics.

Results and discussion

Influence of the error threshold for DAC

In this section, we will demonstrate the influence of mechanism reduction error threshold value ε_{DAC} on the performance of DAC expedited supersonic combustion simulation using DRGEP mechanism reduction method. Figure 3 presents the time-averaged pressure field predicted by DAC simulations with various threshold values for a qualitative comparison.

In consideration of the uncertainty in experiment measurement, simulation with the corresponding detailed ethylene chemical mechanism was conducted and serves as the baseline in the present work to offer the exhaustive thermochemical details. As shown in Figure 3e, the fuel and air streams undergo expansion and compression, respectively, after

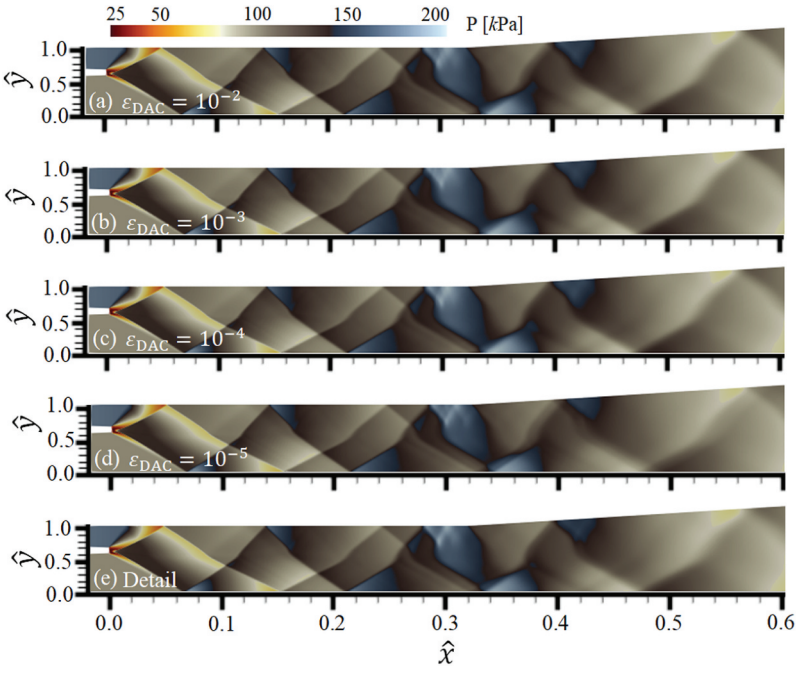

Figure 3. Comparison of time-averaged pressure contours between DAC simulations with various error threshold values against simulation resultobtained with detailed mechanism (DI).

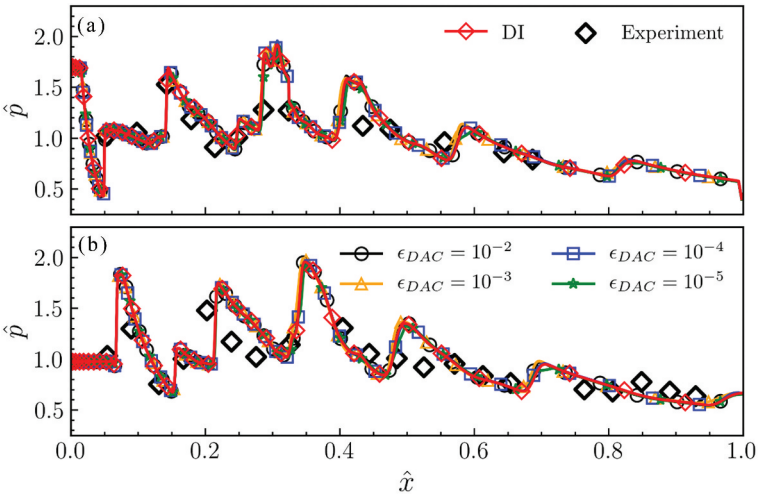

Figure 4. Experimental validation for DAC simulations with various error threshold values (a) upper wall and (b) lower wall.

impinging upon each other. The subsequent expansion wave and oblique wave reflect from the upper and bottom walls and then interact at the location around $\hat{x} = 0.105$. With combustion heat release, the shock wave is strengthened and impinges on the upper wall at around $\hat{x} = 0.282$ leading to a local high-pressure region. Generally, the four simulations with various error threshold values faithfully reproduced the pressure contour and associated wave pattern.

Wall pressure predictions with various error threshold values ε_{DAC} are compared against the experimental data in Figure 4. It is shown that the pressure on the upper wall promptly decreases at the combustor inlet, whereas incidence oblique shock wave on the lower wall increases the local pressure abruptly. After several times of inflections and wave-wave interactions, the strength of the oblique shock wave gradually attenuates as approaching the combustor exit. Quantitatively, pressure distribution on both upper and bottom walls predicted by four levels of ε_{DAC} are indiscernible, and the average relative errors compared to that predicted by detailed mechanism are within 0.2%. Especially, the four simulations with a wide range of ε_{DAC} all faithfully capture the slight pressure decline at $\hat{x} = 0.3$.

To evaluate the accuracy of various ε_{DAC} in predicting the combustor global combustion efficiency, mass fraction profiles of H_2O, CO_2 and CO as well as the temperature profile are probed at the combustor exit as shown in Figure 5. Overall, numerical simulations with various ε_{DAC} values reproduce similar tendency as the detailed mechanism approach for both species and temperature distributions. However, it can be observed that with relatively large ε_{DAC} values, the DAC simulations over predict the peak value of CO mass fraction compared with that by DI calculation in the reacting shear layer as indicated in Figure 5b. Further, with the refinement of the error threshold values, the relative error incurred by DAC simulation decreases.

Since the discrepancies amongst various reduction error threshold values are relatively small, the relative errors in predicting the maximum value for each individual physical property are quantified and summarized in Table 2. It can be found that the relative errors

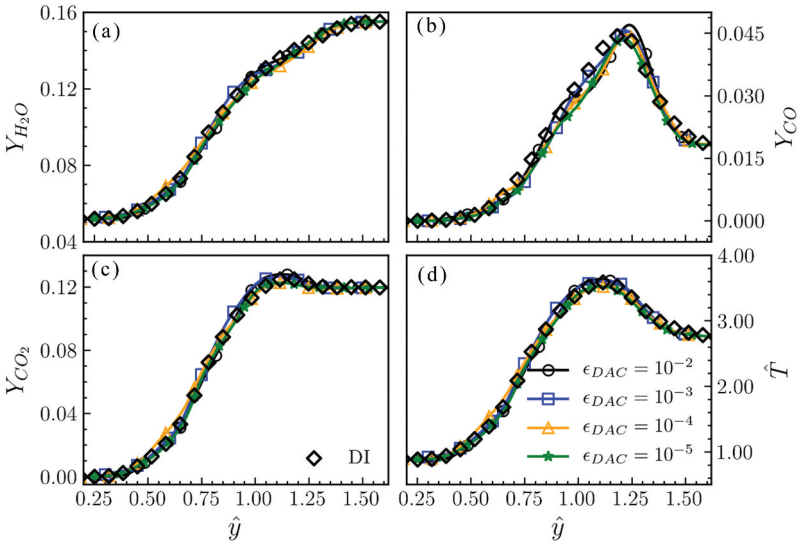

Figure 5. Comparison of time-averaged profiles at the combustor exit predicted under various ε_{DAC} against direct integration with detailed mechanism for (a) mass fraction of H_2O, (b) mass fraction of CO, (c) mass fraction of CO_2, and (d) temperature.

Table 2. Relative errors for maximum value prediction by DAC simulation with DRGEP method under various error threshold values.

	$\varepsilon_{DAC} = 10^{-2}$	$\varepsilon_{DAC} = 10^{-3}$	$\varepsilon_{DAC} = 10^{-4}$	$\varepsilon_{DAC} = 10^{-5}$
ε_{H2O}^{max}	0.000	0.000	0.000	0.000
ε_{CO}^{max}	0.018	0.055	0.003	0.018
ε_{CO2}^{max}	0.022	0.012	0.011	0.021
ε_{T}^{max}	0.014	0.005	0.005	0.017

incurred by DAC simulations manifest a non-monotonic behavior regarding the ε_{DAC}, and the relative error exceeds 15% when ε_{DAC} is greater than 10^{-4}. This indicates that for practical scramjet engine simulations with DAC, it is more appropriate to keep the ε_{DAC} within 10^{-4}.

In our previous study (Wu et al. 2018), it was suggested that the static skeletal mechanism was incapable to accurately reproduce the flame stabilization location even with elaborately devised skeletal mechanism. After coupling the mechanism reduction with fluid flow simulation, the DAC method manifested its superiority in flame dynamic prediction. As shown in Figure 6a-c, two local regions with higher OH concentrations reside around $\hat{x} =$ 0.31 and 0.41, which are almost identical to that predicted by the detailed mechanism in Figure 6e. The simulation with the coarsest error threshold value of $\varepsilon_{DAC} = 10^{-2}$also well reproduces the streamwise locations of these two regions, nevertheless with higher OH concentration quantitatively in the upstream location.

To further scrutinize the prediction accuracy of various mechanism reduction error threshold values, mass fraction of OH are sampled and compared to that simulated with detailed mechanism. The sampling locations are $\hat{x}_A = 0.1$, $\hat{x}_B = 0.2$, $\hat{x}_C = 0.3$ and $\hat{x}_D = 0.4$

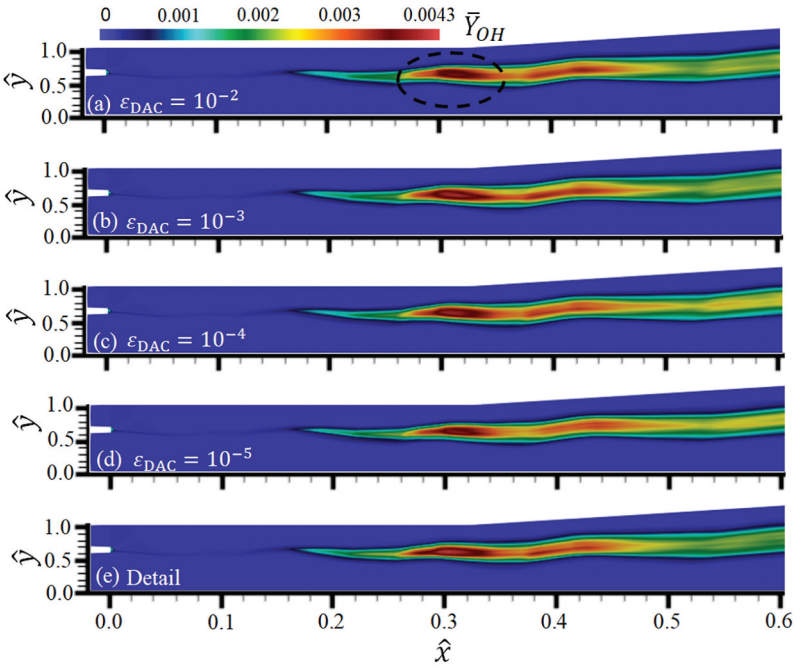

Figure 6. Comparison of time-averaged OH mass fraction contours between DAC simulations with different error threshold values against direct integration.

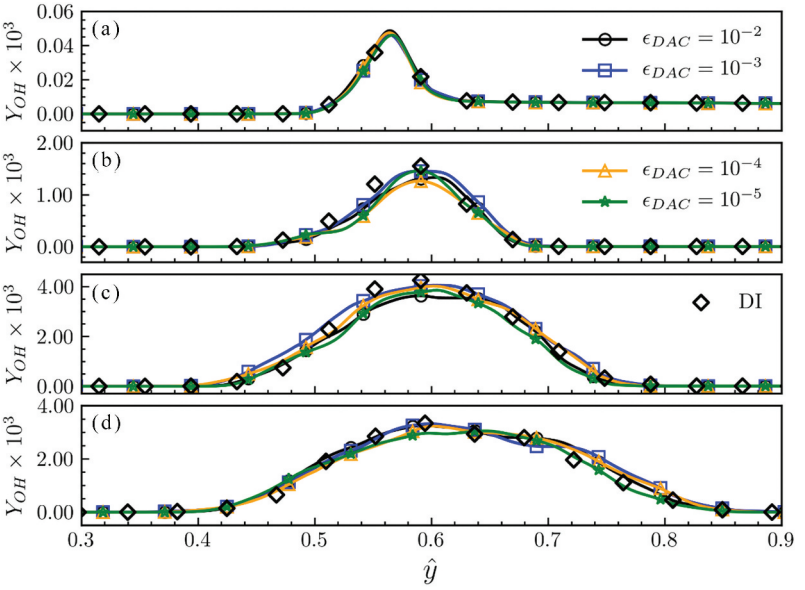

Figure 7. Comparison of the time-averaged profiles of OH mass fraction predicted under various ε_{DAC} against direct integration with detailed mechanism at different streamwise locations: (a) location A, (b) location B, (c) location C, and (d) location D.

respectively along the combustor centerline, which are denoted in Figure 1. Figure 7 displays the time-averaged profiles of OH mass fraction predicted under various ε_{DAC} at different streamwise locations. At location A where chemical reactions initiate, the DAC simulations with various levels of ε_{DAC} produce almost identical Y_{OH} distribution. At locations B, the discrepancies among predictions become noticeable, wherein DAC simulations with $\varepsilon_{DAC} = 10^{-2}$ and 10^{-4} under predict the peak value of Y_{OH}. Further downstream, the discrepancies between DAC simulations with various error threshold values gradually fade away, while the simulation with $\varepsilon_{DAC} = 10^{-4}$ still attains favorable agreement with the DI calculation.

To assess the accuracy of various ε_{DAC} values in scramjet engine performance evaluation, quasi one-dimensional analyses were performed based on the simulation results. The one-dimensional distributions of physical properties are calculated by mass-weighted averaging on cross-section at each streamwise location. From Figure 8, simulations with four various error threshold values yield indistinguishable streamwise distributions regarding mass fraction of representative species. It is worth noting that the heat release distribution is decisive for pressure distribution and in turn the propulsion performance of the scramjet engine. As can be observed from Figure 8d that the simulations with DAC method compare

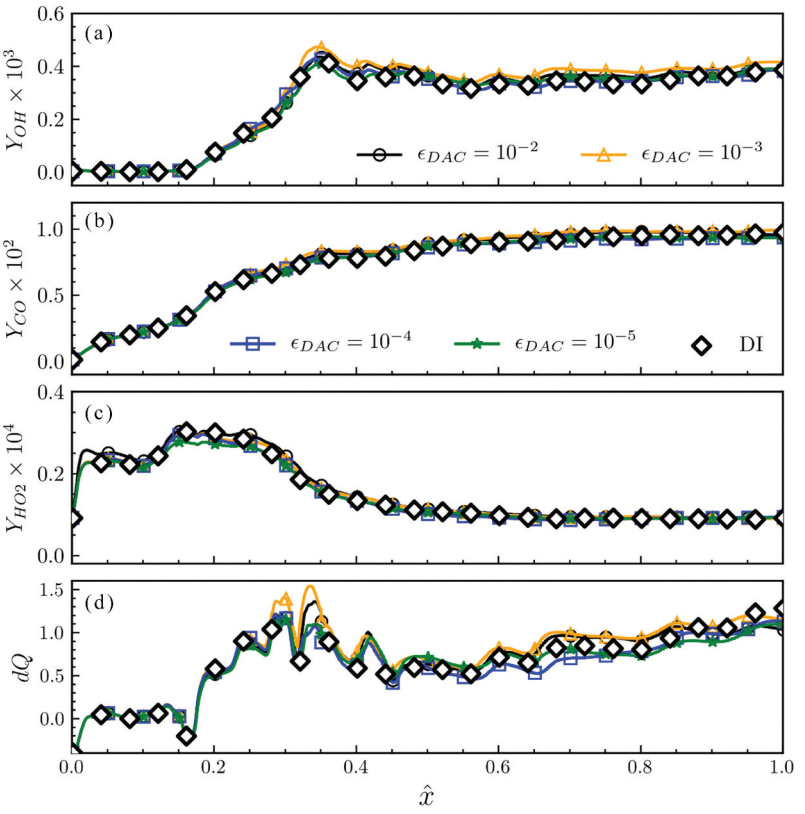

Figure 8. Comparison of the one-dimensional profiles predicted by various ε_{DAC} against direct integration with detailed mechanism for: (a) OH mass fraction, (b) CO mass fraction, (c) HO_2 mass fraction, and (d) heat release rate.

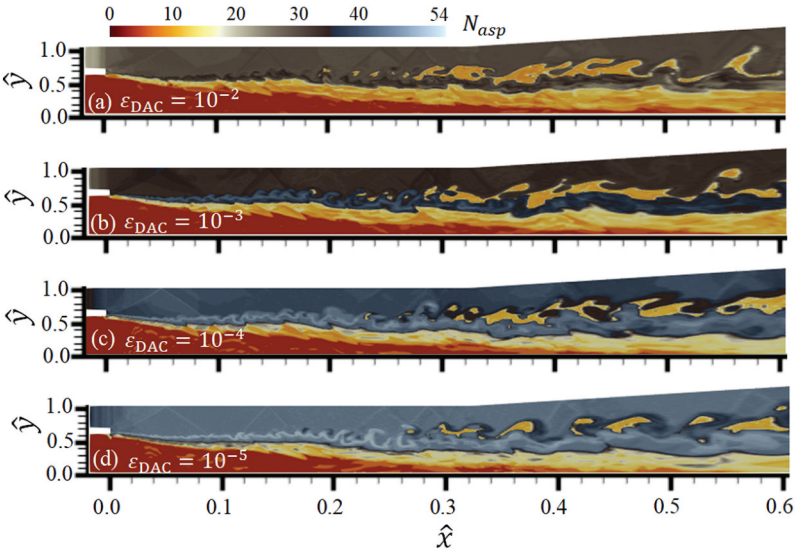

Figure 9. Contour plots of the number of active species N_{asp} obtained under various ε_{DAC}.

favorably with the direct integration of detailed chemistry when relatively small ε_{DAC} is employed, while large discrepancy will occur under coarse ε_{DAC} values. This again confirms that to accurately predict the engine performance, the ε_{DAC} value should not exceed 10^{-4}.

The aforementioned discussions concern more on the prediction accuracy with various error threshold values within the framework of DAC; however for high-fidelity simulation, the computational efficiency is equally important. Figure 9 displays the instantaneous number contours of active species obtained using various reduction error thresholds. Figure 9a exemplifies the spatial distribution of local reactivity in the combustor, which is characterized by the number of active species obtained by DRGEP method based on local and instantaneous thermochemical conditions. Based on the distribution of N_{asp}, the entire combustor can be roughly divided into three regions, the fuel-rich region (mainly the fuel stream) near the upper wall, the fuel-lean region (mainly the air stream) near the bottom wall, and the reacting shear layer between these two streams. In the fuel-rich region, the chemical reactivity is predominantly controlled by the fuel pyrolysis reaction under intermediate temperature, wherein the fuel converts into smaller hydrocarbons or radicals and involves many more reactions than in the combustion stage (Glassman, Yetter, and Glumac 2004). On the contrary, chemical reactions in the fuel-lean region can be faithfully represented by a small number of active species as the reaction can hardly occur in the vitiated air stream. In the shear layer, the mixing between mixtures and subsequent reaction occurs around a favorable local equivalence ratio, which yields high combustion temperature and can be characterized by active species in a number of 10 to 20. Regarding the spatial distribution of the active species, the DAC simulation with $\varepsilon_{DAC} = 10^{-4}$ resembles that with $\varepsilon_{DAC} = 10^{-5}$ both qualitatively and quantitatively. However, when increases the ε_{DAC} value, the number of active species in fuel rich stream decreases remarkably, whereas decreases of N_{asp} in the vitiated air stream is relatively small.

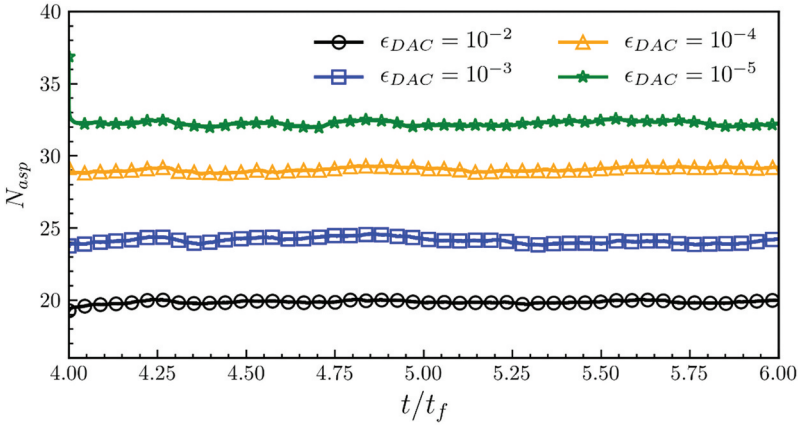

Figure 10. Time history of the spatial-averaged active species number in four DAC simulations under various ε_{DAC}.

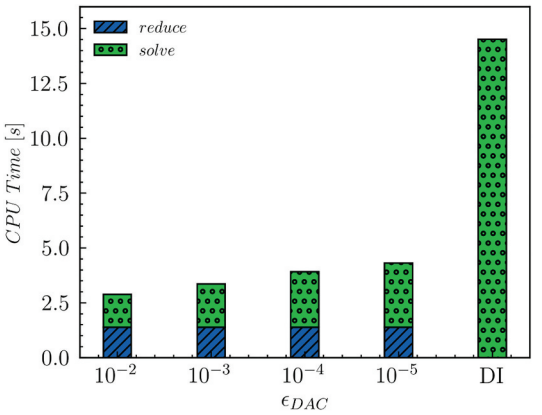

Figure 11. Cpu time for mechanism reduction and subsequent ODE solving with various ε_{DAC}.

For a quantitative comparison, the domain averaged number of active species N_{asp} is exhibited in Figure 10 which is a direct representative of the overall computational load. It is shown that with tighter error threshold ε_{DAC}, the more active species are retained in the on-the-fly reduced chemical mechanisms. With the moderate ε_{DAC} value (10^{-3}), the number of active species is around 24, which achieves a remarkable reduction in species number compared to the detailed one (54 species). We also note that, for each ε_{DAC} value, fluctuation in active species number is always discernable. This indicates that, even in the quasi steady state, the flame stabilization is a highly dynamical process being closely coupled with complex chemical kinetics.

The corresponding computational efficiency comparison is displayed in Figure 11. The computational speedup factor is calculated as

$$\chi_{su} = \frac{\tau_{DI}}{\tau_{DAC}} \tag{16}$$

where τ_{DI} and τ_{DAC} are the mean CPU times over simulations with detailed mechanism and dynamic adaptive method, respectively.

Regarding the computational efficiency, Figure 11 shows the CPU times for each DAC simulation with various ε_{DAC}. Specifically, the CPU time consumption in chemical reaction calculation for DAC approach can be divided into two main components, including the time for mechanism reduction and the time for solution of the subsequent ODE of the skeletal mechanism. It is interesting to find that the computational overhead incurred by the mechanism reduction process is almost unchanged under a wide range of ε_{DAC}. The computational speedup is more likely to be squeezed from the computational time for a size-reduced stiff ODE system. The simulation with DRGEP and $\varepsilon_{DAC} = 10^{-3}$ achieves a computational speedup factor $\chi_{su} = 3.71$, while 4.33 and 3.19 folds of speedup factors are obtained with coarser and tighter error threshold values of 10^{-2} and 10^{-4}, respectively.

Based on the above discussion, the DAC simulation with $\varepsilon_{DAC} = 10^{-4}$ performs favorably regarding both the numerical accuracy and computational efficiency. Thus, the investigation of other influential factors including the mechanism reduction method and the SIS will retain this configuration.

Synergetic influence of mechanism reduction method and error threshold

In this section, we will demonstrate the influence of mechanism reduction methods under error threshold value of $\varepsilon_{DAC} = 10^{-4}$on the DAC simulation of supersonic combustion. Figure 12 presents DAC synergized simulations with four mechanism reduction methods including DRG, DRGEP, DAC-L and PFA. This proves the efficacy of various mechanism

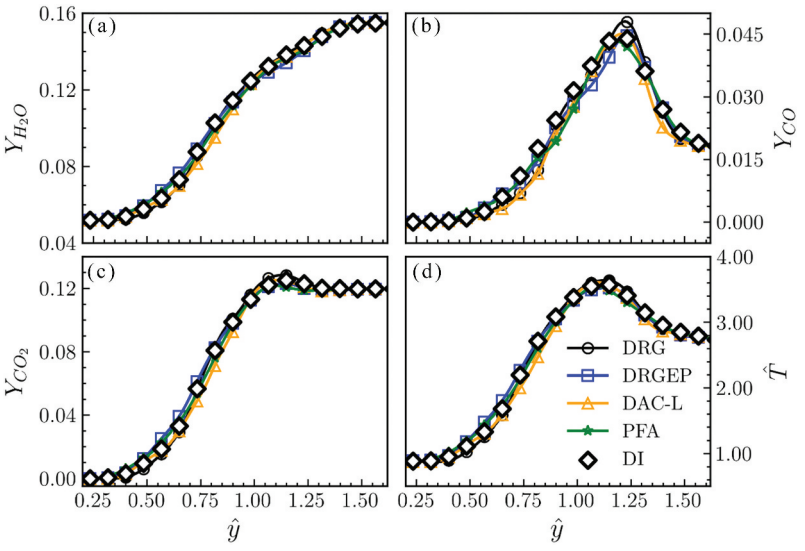

Figure 12. Comparison of the time-averaged profiles at the combustor exit predicted by various mechanism reduction methods against direct integration for (a) mass fraction of H_2O, (b) mass fraction of CO, (c) mass fraction of CO_2 and (d) temperature.

Table 3. Relative errors for maximum value prediction with various mechanism reduction methods.

	DRG	DRGEP	DAC-L	PFA
ε_{H2O}^{max}	0.000	0.000	0.000	0.000
ε_{CO}^{max}	0.080	0.003	0.012	0.022
ε_{CO2}^{max}	0.026	0.011	0.000	0.026
ε_{T}^{max}	0.015	0.005	0.006	0.012

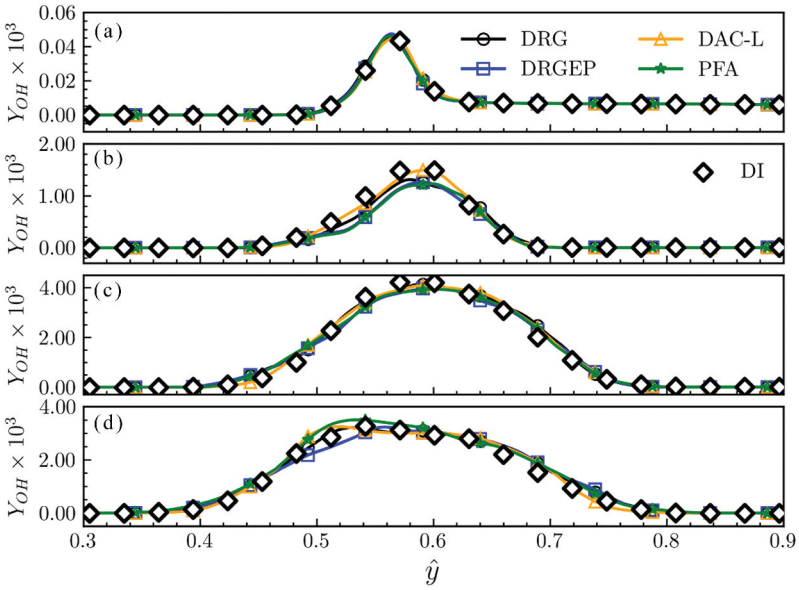

Figure 13. Comparison of the time-averaged profiles of OH mass fraction predicted by various mechanism reduction methods against direct integration with detailed mechanism at different streamwise locations: (a) location A, (b) location B, (c) location C and (d) location D.

reduction methods in dynamically adjusting the local representative skeletal mechanism based on instantaneous and local thermochemical properties, wherein all the DAC simulation could qualitatively reproduce the species' and temperature' distributions at the combustor exit with reasonable accuracy.

Table 3 summarizes the relative errors for maximum value prediction by DAC simulation with various mechanism reduction methods. It can be found that the DAC-L method attains the best prediction accuracy in both temperature and species concentrations. Despite it considers formation and consumption fluxes of species at multiple generations in species dependency calculation, the PFA method incurs the largest relative error in predicting species mass fractions of CO and CO_2.

In Figure 13a, OH species mainly concentrate around the shear layer between two streams, however in very low mass fraction (Y_{OH} 10^{-5}), which indicates the initiation of oxidation reactions. At location B as shown in Figure 13b, the mass fraction of OH increases significantly and reaction zone becomes wider. Among the four mechanism reduction methods, DAC-L and DRGEP methods show reasonable good agreement with the detailed mechanism, while DRG and PFA methods slightly underpredict the peak value of OH mass

Table 4. Active species and removed reactions in the instantaneous locally reduced skeletal mechanism at location B for different mechanism reduction methods.

Active Species	
(#active species in common) H, O2, OH, O, H2, H2O, HO2, H2O2, CO, CO2, HCO, CH3, CH4, CH2O, *T*-CH2, S-CH2, C2H4, CH3O, C2H5, C2H6, CH, C2H2, C2H4OOH, C2H3, CH2CHO, C2H4O, HCCO, CH2CO, C2H, CH2OH, CH3OH, CH3CHO, CH3CO, C2H5OH, CH2CH2OH, CH3CHOH, CH3CH2O, C3H4, C3H3, C3H5, C3H6, C3H8, I-C3H7, N-C3H7	
DAC	C3H6OOH, SC4H9, C4H8, SC4H9O2
DRG	C3H6OOH, PC4H9, SC4H9, C4H8, SC4H9O2
DRGEP	C4H8
PFA	C3H6OOH, SC4H9, C4H8, SC4H9O2
Removed Reactions	
(#removed reactions in common) R244: C3H6OOH+O2=OC3H5OOH+OH R245: OC3H5OOH=CH2CHO+CH2O+OH R246: PC4H9=C2H5+C2H4 R253: PC4H9+O2=C4H8OOH1-3 R254: C4H8OOH1-3=C4H8+HO2 R255: C4H8OOH1-3+O2=NC4KET13+OH R256: NC4KET13=N-C3H7+CO2+OH	
DAC	R242: N-C3H7+O2=C3H6OOH R243: C3H6OOH=C3H6+HO2 R247: SC4H9=C3H6+CH3 R250: SC4H9+O2=SC4H9O2 R251: SC4H9O2=C4H8+HO2 R252: PC4H9+O2=C4H8+HO2
DRG	R252: PC4H9+O2=C4H8+HO2
DRGEP	R242: N-C3H7+O2=C3H6OOH R243: C3H6OOH=C3H6+HO2 R247: SC4H9=C3H6+CH3 R250: SC4H9+O2=SC4H9O2 R251: SC4H9O2=C4H8+HO2 R252: PC4H9+O2=C4H8+HO2
PFA	R91: C2H4OOH+O2=OC2H3OOH+OH R92: OC2H3OOH =CH2O+HCO+OH

fraction. At location C, all mechanism reduction methods produce similar results as the detailed mechanism method. Further downstream, at location D, OH mass fraction calculated by DRGEP method again shows good agreement with that by detailed mechanism. However, the PFA method overshoots the peak value in OH mass fraction at the fuel lean side.

As the disparities between the simulations results using different mechanism reduction methods are more remarkable at location B, a more in-depth analysis is conducted with the local thermochemical information. Since the chemical reaction initializes there, a large number of active species is needed to characterize the local combustion. In Table 4, there are 44 active species shared by all the four mechanism reduction methods, while the DRGEP method only needs one more species C_4H_8. While the active species of DRG and PFA methods are all the same, they remove the R252 and R91–92, respectively, in addition to the common removed reactions. It is also interesting that the DAC-L and DEGEP methods remove the same reactions, nonetheless their active species differ. This reflects the

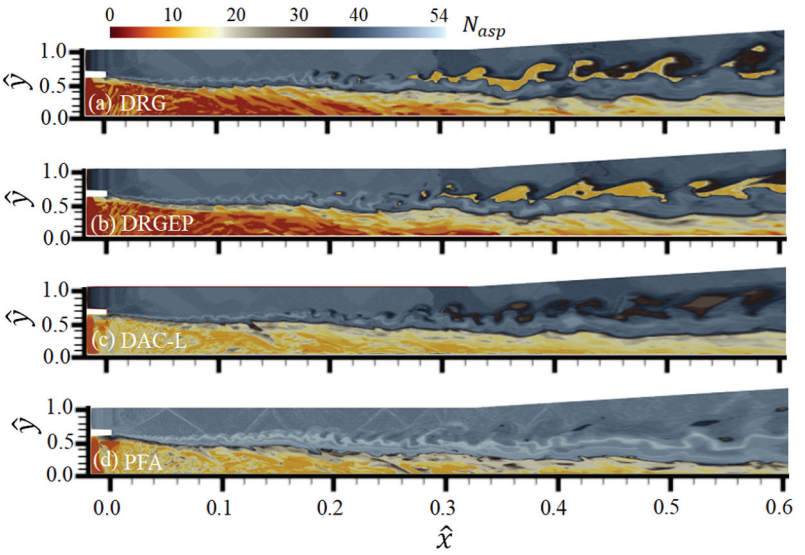

Figure 14. Contour plots of the number of active species N_{asp} obtained using various mechanism reduction methods.

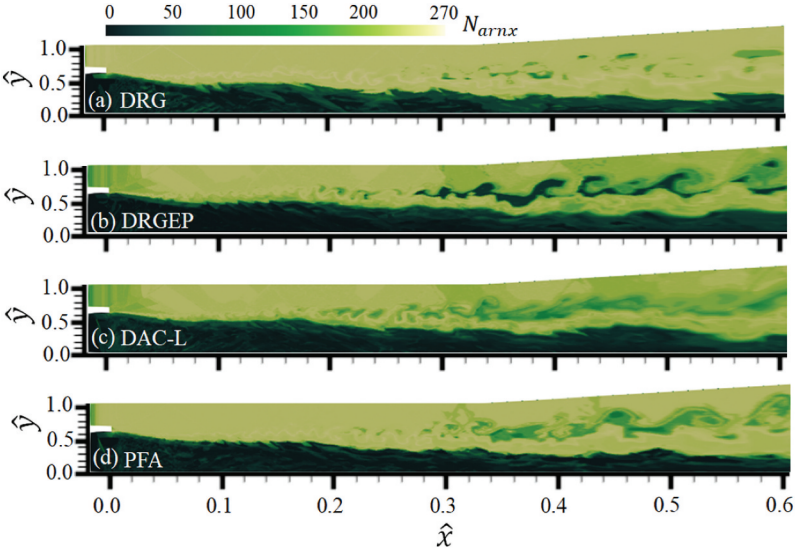

Figure 15. Contour plots of the number of active reactions N_{arxn} obtained using various mechanism reduction methods.

complexity of chemical reaction network, wherein the reduction in species is not necessarily means reaction removal.

Regarding the spatial distribution of the active species in Figure 14, the DRGEP method resembles the DRG method both qualitatively and quantitatively. In the simulation with the DAC-L method, the number of active species in the fuel-lean region and the reacting shear layer is slightly larger than that in the DRG and DRGEP methods. However, a remarkable

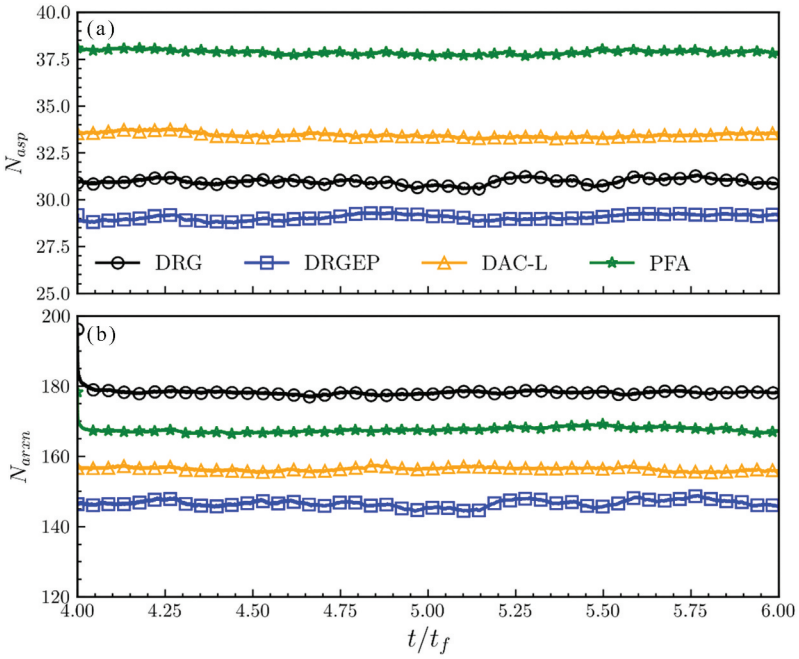

Figure 16. Time history of the spatial-averaged (a) active species and (b) reaction numbers in four DAC simulations with various mechanism reduction methods.

difference can be found in the PFA method when compared to the other three counterparts, as the fuel-rich region possesses around 44 active species, while the number of active species approximates the detailed mechanism (54 species) in the reacting shear layer.

Figure 15 displays the corresponding number of active reaction N_{arxn} obtained using various mechanism reduction methods. It can be observed that the general distribution of the active reactions number is consistent with that of the active species. However, the DRG method retains the largest number of reactions compared to the other three methods. Although the PFA method has more active species number, its associated number of active reactions is relatively smaller than that in the DRG method. The DRGEP method reduces the active reactions in the high temperature reactive shear layer in the downstream location to the largest extent.

For quantitative comparison, the temporal evolution of the domain averaged active species number is exhibited in Figure 16a. The DRGEP method produces the least number of active species, which is consistent with the observation in Figure 14. In the simulation with the DAC-L method, the resultant N_{asp} is around 33.5, which is relatively larger than that produced by DRG and DRGEP methods. This should be attributed to the fact that the influence of removing a species group is neglected in the DAC-L method compared to DRGEP method. The DAC simulation employing the PFA method results in a much larger N_{asp} compared to the other three methods. The associated numbers of active reactions are also shown in Figure 16b. Compared to the evolution of active species, the only exception is the N_{arxn} of DRG method which is the largest among all the four methods. This may be attributes to the fact that the DRG method is less efficient in elemental reactions reduction.

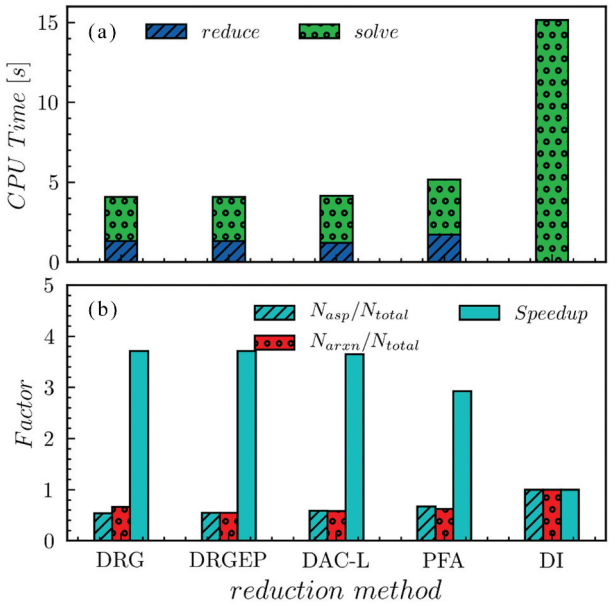

Figure 17. Number of active species and reactions along with speed-up factors in four DAC simulations with various mechanism reduction methods.

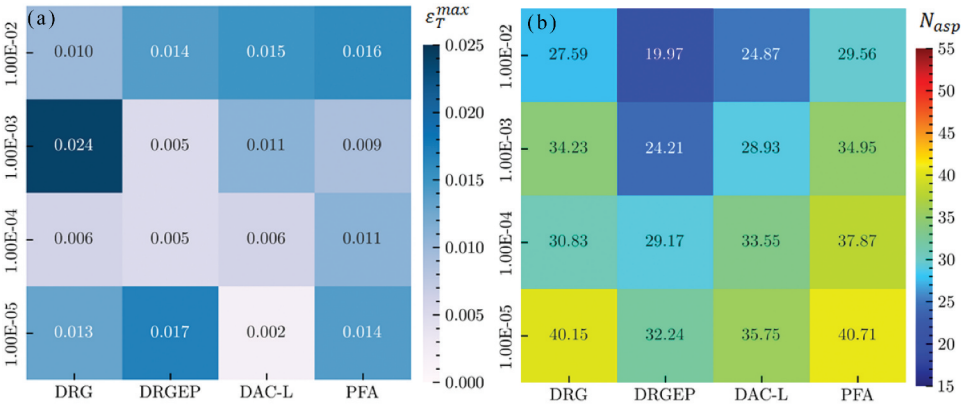

Figure 18. A comprehensive sweep over all the combinations of the mechanism reduction methods and levels of reduction error threshold values: (a) the relative error of maximum temperature prediction at the combustor exit and (b) number of the domain-averaged active species.

As for the overall computational efficiency, as shown in Figure 17, the CPU time for solving the ODE on a reduced-scale system consumes just a quarter of the original calculation with the detailed chemistry (DI case), while the mechanism reduction incurs overhead which is about 30% of the total computational load. Therefore, the overall computational speed-up factor achieves 2.82 to 3.72 depending on the adopted mechanism reduction method.

It is worth noting that the definition of the threshold is different for the different mechanism reduction methods. So it is not fair to compare them keeping the same

threshold values. Thus, we conducted as sweep across all possible combinations of mechanism reduction methods and error threshold values to investigate their synergetic effect. As present in Figure 18, the DAC simulation with DRGEP and $\varepsilon_{DAC} = 10^{-4}$ yields the best balance between the computational cost and numerical accuracy.

Influence of the search initiating species

Further, from the essence of the DRG-based mechanism reduction method, the SIS is decisive to the resultant reaction network as the related relation graph is constructed starting from the SIS. In the present work, two typical SIS sets including the stable reactant combination as C_2H_4, O_2 and N_2 denoted as Stable-SIS, and C_2H_4 as well as intermediate species such as CO, HO_2 which is denoted as inter-SIS. It should be noted that the DRGEP-based DAC simulations in this section are conducted under a relative tight error threshold of 10^{-4}.

Figure 19 demonstrates the influence of the SIS on the prediction of species mass fractions and temperature at the combustor exit. Analogous to those in Figures 5 and 12, the most notable discrepancy is again found in the CO mass distribution. As summarized in Table 5, the stable-SIS induces 0.8% relative error in CO prediction, which is nearly 0.5% higher than that by Inter-SIS simulation. Furthermore, the simulation with Inter-SIS

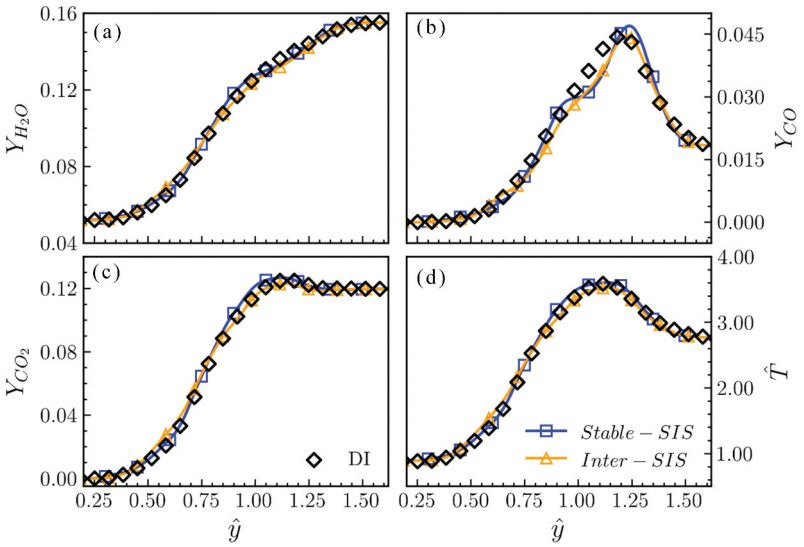

Figure 19. Comparison of the time-averaged profiles at the combustor exit predicted under various SIS against direct integration for (a) mass fraction of H_2O, (b) mass fraction of CO, (c) mass fraction of CO_2 and (d) temperature.

Table 5. Relative errors for maximum value prediction by DAC simulation with DRGEP method and various SIS combinations.

	ε_{H2O}^{max}	ε_{CO}^{max}	ε_{CO2}^{max}	ε_{T}^{max}
Stable-SIS	0.000	0.008	0.024	0.018
Inter-SIS	0.000	0.003	0.011	0.005

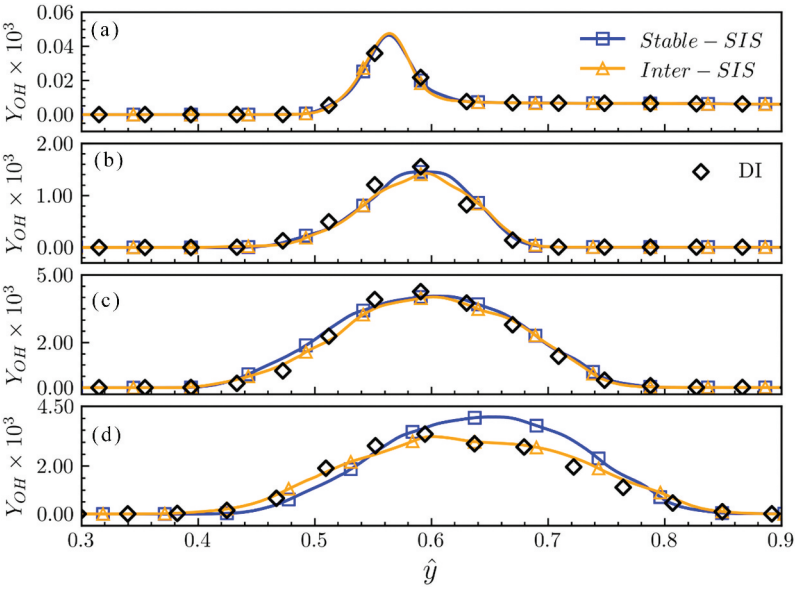

Figure 20. Comparison of the time-averaged profiles of OH mass fraction predicted under various SIS sets against direct integration at different streamwise locations: (a) location A, (b) location B, (c) location C and (d) location D.

achieves much lower relative errors compared to those predicted by stable-SIS regarding CO_2 mass fraction and temperature distributions.

As can be seen from Figure 20a–c, the influences of SIS at upstream locations are marginal compared to that induced by mechanism reduction method and error threshold value. However, the effect of SIS becomes more pronounced at downstream location D, where the Stable-SIS simulation significantly overpredicts the maximum value of OH mass fraction. By parsing through the directed relation graph constructed at this location, we summarized the active species and removed chemical reactions in Table 6. We found that the number of active species in Stable-SIS is smaller than that in the Inter-SIS case, where more species with carbon number greater than 3 are removed in Stable-SIS. It is also recognized that most of the additional removed reactions in the Stable-SIS involve OH, H, and HO_2. Hence, the consumption rate of the OH radical at location D is attenuated compared to that based on Inter-SIS compared to the Stable-SIS case.

The contours of active species number N_{asp} obtained with Inter-SIS and Stable-SIS are displayed in Figure 21. It is obvious that the N_{asp} of Stable-SIS is smaller than that obtained by Inter-SIS in the entire combustor including both the fuel-rich and the fuel-lean streams. Especially, in the fuel-rich stream, the DAC simulation with Stable-SIS needs 30–40 active species while that with Inter-SIS requires another 10 more species. This tendency is further quantified in Figure 22 showing that the DAC simulation with Inter-SIS overall requires around 29 species, and the Stable-SIS simulation needs 24 active species. Correspondingly, the Inter-SIS is more computational demanding than the Stable-SIS as displayed in Figure 23. It is worth noting that the computational overhead for mechanism reduction is

Table 6. Active species and removed reactions in the instantaneous locally reduced skeletal mechanism at location D for different SIS.

Active Species		
(#active species in common) H, O2, OH, O, H2, H2O, HO2, H2O2, CO, CO2, HCO, CH3, CH4, CH2O, *T*-CH2, S-CH2, C2H4, CH3O, C2H5, C2H6, CH, C2H2, C2H4OOH, C2H3, CH2CHO, C2H4O, HCCO, CH2CO, C2H, CH2OH, CH3OH, CH3CHO, CH3CO, C2H5OH, CH3CH2O, C3H4, C3H3, C3H5, C3H6		
Inter-SIS	CH2CH2OH, CH3CHOH, C3H8, I-C3H7, N-C3H7	
Stable-SIS	N-C3H7, C4H8	
Removed Reactions		
(#remove reactions in common) R242: N-C3H7+O2=C3H6OOH R243: C3H6OOH=C3H6+HO2 R244: C3H6OOH+O2=OC3H5OOH+OH R245: OC3H5OOH=CH2CHO+CH2O+OH R246: PC4H9=C2H5+C2H4 R247: SC4H9=C3H6+CH3 R250: SC4H9+O2=SC4H9O2 R251: SC4H9O2=C4H8+HO2 R252: PC4H9+O2=C4H8+HO2 R253: PC4H9+O2=C4H8OOH1-3 R254: C4H8OOH1-3=C4H8+HO2 R255: C4H8OOH1-3+O2=NC4KET13+OH R256: NC4KET13=N-C3H7+CO2+OH		
Inter-SIS	-	
Stable-SIS	R168: C2H5OH+OH=CH2CH2OH+H2O R169: C2H5OH+OH=CH3CHOH+H2O R171: C2H5OH+H=CH2CH2OH+H2 R172: C2H5OH+H=CH3CHOH+H2 R174: C2H5OH+O=CH2CH2OH+OH R175: C2H5OH+O=CH3CHOH+OH R177:C2H5OH+CH3=CH2CH2OH+CH4 R178: C2H5OH+CH3=CH3CHOH+CH4 R180:C2H5OH+HO2=CH3CHOH+H2O2 R181:C2H5OH+HO2=CH2CH2OH+H2O2 R184: C2H5+HO2=CH3CH2O+OH R192: CH3CHOH+O2=CH3CHO+HO2 R193: CH3CHOH+O=CH3CHO+OH R194: CH3CHOH+H=C2H4+H2O R195: CH3CHOH+H=CH3+CH2OH R196: CH3CHOH+HO2=CH3CHO+2OH	R197:CH3CHOH+OH=CH3CHO+H2O R198: CH3CHOH=CH3CHO+H R226: C3H8+O2=I-C3H7+HO2 R227: C3H8+O2=N-C3H7+HO2 R228: C3H8+H=I-C3H7+H2 R229: C3H8+H=N-C3H7+H2 R230: C3H8+O=I-C3H7+OH R231: C3H8+O=N-C3H7+OH R232: C3H8+OH=N-C3H7+H2O R233: C3H8+OH=I-C3H7+H2O R234: C3H8+HO2=I-C3H7+H2O2 R235: C3H8+HO2=N-C3H7+H2O2 R236: I-C3H7+C3H8=NC3H7+C3H8 R237: C3H6+H=I-C3H7 R238: I-C3H7+O2=C3H6+HO2

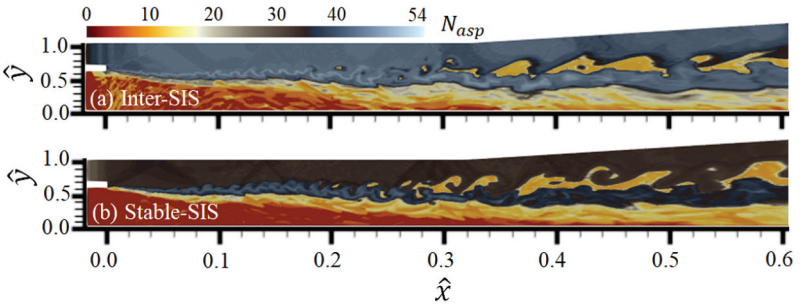

Figure 21. Contour plot of the number of active species N_{asp} obtained with Inter-SIS and Stable-SIS, respectively.

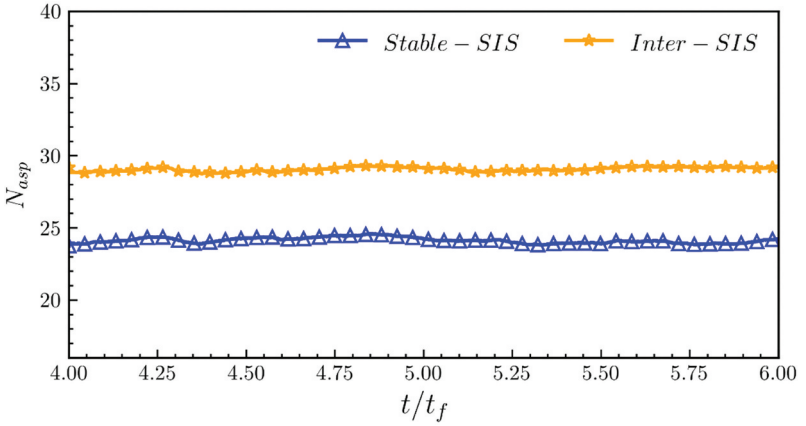

Figure 22. Time history of the spatial-averaged active species number in two DAC simulations under various SIS.

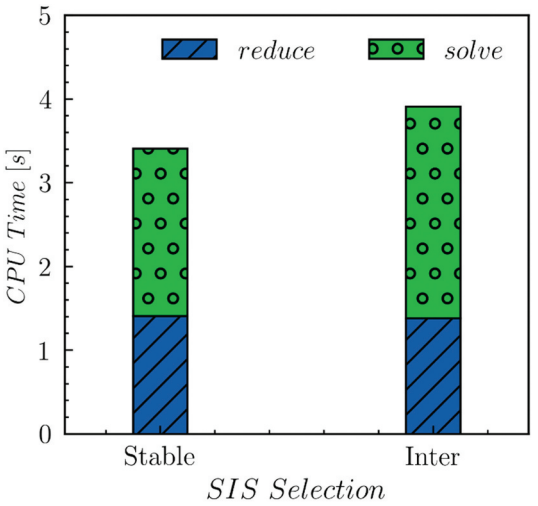

Figure 23. Cpu time for mechanism reduction and subsequent ODE solving with various SIS.

comparable for both SIS combinations, while the Inter-SIS needs 15% more CPU time to solve the resultant stiff-ODE.

Concluding remarks

The DAC augmented large eddy simulation of supersonic combustion in scramjet engine was realized in this study. The influences of mechanism reduction method, mechanism reduction threshold value, and SIS were systematically evaluated in a unified framework. Numerical validation was first conducted against experimental measurement and the simulation results obtained by direct integration with detailed mechanism were employed to assess the accuracy and computational efficiency of DAC simulations with various configurations.

Based on our comprehensive assessment, four mechanism reduction methods are all found to be adequate for wall pressure and combustors global metrics predictions. However, for detailed flame stabilization characteristics, the DRG, DEGEP, and DAC-L methods attain comparable prediction accuracy in radicals distribution, while the prediction by PFA method shows relatively large relative error. Among all these four mechanism reduction methods, the DRGEP method obtains relatively better balance between the numerical accuracy and computational efficiency, whereas the PFA is the most computational demanding one.

As the mechanism reduction error threshold value increases, the relative errors in predicting intermediate species also increase. It is found that the computational overheads for mechanism reduction under various error threshold values remain almost unchanged, and the overall computational efficiency is mainly determined by the CPU time for solving the size-reduced skeletal mechanisms. And for high-fidelity simulation of supersonic combustion, it is necessary to keep the ε_{DAC} within 10^{-4} to ensure that the relative error in radical mass fraction prediction does not exceed 15%. Regarding the SIS, the stable species combination including fuel, O_2 and N_2 produces larger relative error in radicals' concentration prediction than the combination including fuel and intermediate species HO_2 and CO. However, the latter is less computational efficient than the former as it needs 15% more CPU time to solve the stiff ODE system of the resultant skeletal mechanism.

Acknowledgement

This work was supported by National Key Project (Grant No. GJXM92579). The authors are also grateful to the National Supercomputer Center in Tianjin for providing the computational resource.

Disclosure statement

No potential conflict of interest was reported by the author(s).

Funding

The work was supported by the National Key Project [GJXM92579].

ORCID

Francesco Contino http://orcid.org/0000-0002-8341-4350

References

Bertin, J. J., and R. M. Cummings. 2003. Fifty years of hypersonics: Where we've been, where we're going. *Prog. Aeosp. Sci* 39 (6–7):511–36. doi:10.1016/S0376-0421(03)00079-4.

"Chemical-Kinetic Mechanisms for Combustion Applications", S. D. M. w. p., Mechanical and Aerospace Engineering (combustion research). University of California at San Diego. (http://combustion.ucsd.edu).

Contino, F., F. Foucher, P. Dagaut, T. Lucchini, G. D'Errico, and C. Mounaïm-Rousselle. 2013. Experimental and numerical analysis of nitric oxide effect on the ignition of iso-octane in

a single cylinder HCCI engine. *Combust. Flame* 160 (8):1476–83. doi:10.1016/j.combustflame.2013.02.028.

Contino, F., H. Jeanmart, T. Lucchini, and G. D'Errico. 2011. Coupling of in situ adaptive tabulation and dynamic adaptive chemistry: An effective method for solving combustion in engine simulations. *Proc. Combust. Inst* 33 (2):3057–64. doi:10.1016/j.proci.2010.08.002.

Contino, F., J.-B. Masurier, F. Foucher, T. Lucchini, G. D'Errico, and P. Dagaut. 2014. Cfd simulations using the tdac method to model iso-octane combustion for a large range of ozone seeding and temperature conditions in a single cylinder hcci engine. *Fuel* 137:179–84. doi:10.1016/j.fuel.2014.07.084.

Curtis, N. J., K. E. Niemeyer, and C.-J. Sung. 2015. An automated target species selection method for dynamic adaptive chemistry simulations. *Combust. Flame* 162 (4):1358–74. doi:10.1016/j.combustflame.2014.11.004.

Fureby, C. (2012). LES for supersonic combustion. 18th AIAA/3AF International Space Planes and Hypersonic Systems and Technologies Conference, AIAA Paper, Tours, France: American Institute of Aeronautics and Astronautics, AIAA-2012-5979.

Glassman, I., R. A. Yetter, and N. G. Glumac. 2004. *Combustion*, 5th ed., San Diego, California, USA: Academic Press.

Gou, X., Z. Chen, W. Sun, and Y. Ju. 2013. A dynamic adaptive chemistry scheme with error control for combustion modeling with a large detailed mechanism. *Combust. Flame* 160 (2):225–31. doi:10.1016/j.combustflame.2012.10.015.

He, K., I. P. Androulakis, and M. G. Ierapetritou. 2010. On-The-Fly reduction of kinetic mechanisms using element flux analysis. *Chem. Eng. Sci* 65 (3):1173–84. doi:10.1016/j.ces.2009.09.073.

Hitch, B. D., and E. D. Lynch. 2009. Use of reduced, Accurate ethylene combustion mechanisms for a hydrocarbon-fueled Ramjet simulation. AIAA Paper, American Institute of Aeronautics and Astronautics, AIAA-2009-5384.

Karlsson, A. 1995. Modeling auto-ignition, flame propagation and combustion in non-stationary turbulent sprays PHD, Chalmers University of Technology.

Law, C. K., C. J. Sung, H. Wang, and T. Lu. 2003. Development of comprehensive detailed and reduced reaction mechanisms for combustion modeling. *AIAA J.* 41 (9):1629–46. doi:10.2514/2.7289.

Li, Z., M. T. Lewandowski, F. Contino, and A. Parente. 2018. Assessment of on-the-fly chemistry reduction and tabulation approaches for the simulation of moderate or intense low-oxygen dilution combustion. *Energy Fuels* 32 (10):10121–31. doi:10.1021/acs.energyfuels.8b01001.

Liang, L., J. G. Stevens, and J. T. Farrell. 2009a. A dynamic adaptive chemistry scheme for reactive flow computations. *Proc. Combust. Inst* 32 (1):527–34. doi:10.1016/j.proci.2008.05.073.

Liang, L., J. G. Stevens, S. Raman, and J. T. Farrell. 2009b. The use of dynamic adaptive chemistry in combustion simulation of gasoline surrogate fuels. *Combust. Flame* 156 (7):1493–502. doi:10.1016/j.combustflame.2009.02.008.

Lu, T., and C. K. Law. 2005. A directed relation graph method for mechanism reduction. *Proc. Combust. Inst* 30 (1):1333–41. doi:10.1016/j.proci.2004.08.145.

Lu, T., and C. K. Law. 2009. Toward accommodating realistic fuel chemistry in large-scale computations. *Prog. Energy Combust. Sci* 35 (2):192–215. doi:10.1016/j.pecs.2008.10.002.

Molvik, G., J. Bowles, and L. O. C. Huynh. (1992). Analysis of a hydrocarbon scramjet with augmented preburning. 28th Joint Propulsion Conference and Exhibit, AIAA Paper, Nashville, TN, USA: American Institute of Aeronautics and Astronautics, AIAA-1992-3425.

Niemeyer, K. E., C.-J. Sung, and M. P. Raju. 2010. Skeletal mechanism generation for surrogate fuels using directed relation graph with error propagation and sensitivity analysis. *Combust. Flame* 157 (9):1760–70. doi:10.1016/j.combustflame.2009.12.022.

Oluwole, O. O., Z. Ren, C. Petre, and G. Goldin. 2015. Decoupled Species and Reaction Reduction: An error-controlled method for Dynamic Adaptive Chemistry simulations. *Combust. Flame* 162 (5):1934–43. doi:10.1016/j.combustflame.2014.12.012.

Pepiot-Desjardins, P., and H. Pitsch. 2008. An efficient error-propagation-based reduction method for large chemical kinetic mechanisms. *Combust. Flame* 154 (1–2):67–81. doi:10.1016/j.combustflame.2007.10.020.

Potturi, A. S., and J. R. Edwards. 2015. Large-Eddy/reynolds-Averaged Navier–Stokes simulation of cavity-stabilized ethylene combustion. *Combust. Flame* 162 (4):1176–92. doi:10.1016/j.combustflame.2014.10.011.

Shi, Y., L. Liang, H.-W. Ge, and R. D. Reitz. 2010. Acceleration of the chemistry solver for modeling DI engine combustion using dynamic adaptive chemistry (DAC) schemes. *Combust. Theory Model* 14 (1):69–89. doi:10.1080/13647830903548834.

Situ, M., Y. Sun, S. Zhang, and C. Wang. (1999). Investigation of supersonic combustion of hydrocarbon fuel-riched hot gas in scramjet combustor. 35th Joint Propulsion Conference and Exhibit, AIAA Paper, Los Angeles, CA, USA: American Institute of Aeronautics and Astronautics, AIAA-1999-2245.

Sun, W., Z. Chen, X. Gou, and Y. Ju. 2010. A path flux analysis method for the reduction of detailed chemical kinetic mechanisms. *Combust. Flame* 157 (7):1298–307. doi:10.1016/j.combustflame.2010.03.006.

Tosatto, L., B. A. V. Bennett, and M. D. Smooke. 2013. Comparison of different DRG-based methods for the skeletal reduction of JP-8 surrogate mechanisms. *Combust. Flame* 160 (9):1572–82. doi:10.1016/j.combustflame.2013.03.024.

Urzay, J. 2018. Supersonic Combustion in Air-Breathing Propulsion Systems for Hypersonic Flight. *Annu. Rev. Fluid Mech* 50 (1):593–627. doi:10.1146/annurev-fluid-122316-045217.

Wei, H., L. Zhou, H. Zhou, Z. Lu, Z. Ren, and G. M. Goldin. 2017. Toward Efficient Chemistry Calculations in Engine Simulations Through Static Adaptive Acceleration. *Combust. Sci. Technol* 189 (4):623–42. doi:10.1080/00102202.2016.1229312.

Wu, K., F. Contino, W. Yao, and X. Fan. 2018. On the application of tabulated dynamic adaptive chemistry in ethylene-fueled supersonic combustion. *Combust. Flame* 197:265–75. doi:10.1016/j.combustflame.2018.08.012.

Wu, K., W. Yao, and X. Fan. 2017a. Development and fidelity evaluation of a skeletal ethylene mechanism under scramjet-relevant conditions. *Energy Fuels* 31 (12):14296–305. doi:10.1021/acs.energyfuels.7b03033.

Wu, K., P. Zhang, and X. Fan. 2022. On jet-wake flame stabilization in scramjet: A LES/RANS study from chemical kinetic and fluid-dynamical perspectives. *Aerosp. Sci. Technol* 120:107255. doi:10.1016/j.ast.2021.107255.

Wu, K., P. Zhang, W. Yao, and X. Fan. 2017b. Numerical Investigation on Flame Stabilization in DLR Hydrogen Supersonic Combustor with Strut Injection. *Combust. Sci. Technol* 189 (12):2154–79. doi:10.1080/00102202.2017.1365847.

Xie, W., Z. Lu, Z. Ren, and L. Hou. 2017. Dynamic adaptive chemistry via species time-scale and Jacobian-aided rate analysis. *Proc. Combust. Inst* 36 (1):645–53. doi:10.1016/j.proci.2016.07.105.

Yang, H., Z. Ren, T. Lu, and G. M. Goldin. 2013. Dynamic adaptive chemistry for turbulent flame simulations. *Combust. Theory Model* 17 (1):167–83. doi:10.1080/13647830.2012.733825.

Yao, W. 2019. Kerosene-Fueled supersonic combustion modeling based on skeletal mechanisms. *Acta Mech. Sin* 35 (6):1155–77. doi:10.1007/s10409-019-00891-w.

Yoshizawa, A. 1986. Statistical theory for compressible turbulent shear flows, with the application to subgrid modeling. *Phys. Fluids* 29 (7):2152–64. doi:10.1063/1.865552.

Zhong, F., L. Chen, F. Li, X. Zhang, and C.-J. Sung. 2013. Numerical Simulation of Ignition and Combustion of Ethylene in a Supersonic Model Combustor with a Reduced Kinetic Mechanism. *Combust. Sci. Technol* 185 (4):548–63. doi:10.1080/00102202.2012.730080.

Zhou, L., and H. Wei. 2016. Chemistry acceleration with tabulated dynamic adaptive chemistry in a realistic engine with a primary reference fuel. *Fuel* 171:186–94. doi:10.1016/j.fuel.2015.12.055.